Journal of Inclusion Phenomena and Molecular Recognition in Chemistry **21**: 79–112, 1995.

Structural Case Studies of Inclusion Phenomena in Zeolites: Xe in RHO and Stilbene in ZSM-5

JOHN B. PARISE

1. Introduction

Zeolite molecular sieves, firmly established in industry as selective heterogeneous catalysts for cracking, reforming, and separations, have more recently been used as platforms for the inclusion chemistry described in this volume. Their unique structures [1] result in the shape selectivity [2] desirable in both classes of applications. The characterization of the position and orientation of absorbed species, their preferred sorption sites, and their interactions with the host framework are fundamental to a proper understanding of the chemistry of zeolites.

X-Ray, neutron, and electron [3] scattering are recognized as the most appropriate and potentially unambiguous tools available for the study of atomic structure, in both crystalline and non-crystalline materials. These techniques are not expedient, but they are often the most efficacious. Zeolitic materials present a number of special problems in crystallographic investigations [4,5] which become magnified in attempting an accurate description of the structure of zeolite/inclusion complexes. These problems include poor crystallinity, pseudo-symmetry, positional and orientational disorder, and the uncertainty in composition. Fortunately, recent developments in scattering [6-9], spectroscopic [10,11], and molecular modeling techniques [12,13] have mitigated against some of these problems. The latter two techniques are discussed in detail elsewhere in this volume.

1.1 RECENT INNOVATIONS IN X-RAY AND NEUTRON TECHNIQUES

Laboratory-based structural studies will continue to play important roles in developing our understanding of zeolite-inclusion phenomena. However, the advent of more powerful X-ray and neutron sources has provided opportunities to perform experiments revealing a level of detail not available in the laboratory. For example, synchrotron X-ray sources provide bright, tunable beams. This allows the study of smaller single crystals and smaller quantities of powder. The ability to tune energy has made routine X-ray absorption and anomalous scattering measurements [14], which were either laborious or impossible to perform using laboratory-based sources [15]. The high angular resolution available at these sources has aided the ab initio solution of complex structures from

powdered samples [16]. Investigations of structural changes in real time are feasible and one example is discussed in this chapter.

1.1.1 *Single Crystal Studies*

When crystals are suitably sized, homogeneous, and ordered, single crystal crystallography is the most powerful, reproducible, and testable technique for the determination of the structure of zeolite/inclusion complexes. Many single crystal studies have concentrated on the interaction between the organic template species, added in hydrothermal crystallization of molecular sieves, and the framework; a recent review of this work in the aluminophosphate systems is given by Pluth and Smith [17]. Another excellent recent example is the work of Koningsveld and co-workers [18-22]. Carefully prepared single crystals of ZSM-5 [19] were examined and the positions and orientations of absorbed species, along with subtle framework distortions, were determined. One important result from these studies was the comparative ease of detection of pseudo-symmetry in the ZSM-5 system using single crystal techniques; subtle changes in framework symmetry can be extremely difficult to detect using spectroscopies and routine powder diffraction. Studies using single crystal diffraction can provide a confident point of departure for subsequent investigations with powder diffraction [23].

The size range of samples suitable for single crystal diffraction has been decreasing steadily with the availability of brighter laboratory and synchrotron sources. Rotating anode sources operating at 18 kW have been available for some time and have allowed routine data collection on zeolite crystals in the 30 μm size range. Recently, these high power conventional sources have been coupled with area detectors, such as image plates and charge coupled detectors (CCD's). The problems associated with X-ray fluorescence not withstanding, the dynamic range and sensitivity of the former devices make them particularly well-suited to the study of small single crystals of inclusion complexes at low temperatures. For example, we have absorbed a number of gases into 35 μm crystals of zeolite X and have been able to locate density within the channels related to the absorbed species. The data for these studies were collected at 120 K using a 6 kW source and a commercially available imaging-plate system. A full data set was collected in 2 hours raising the possibility of real-time studies involving sorption and desorption as a function of temperature and pressure. With the advent of more powerful conventional and synchrotron sources, and more sensitive detection systems, the line between single crystals and powders continues to blur.

1.1.2 *Powder Diffraction Studies*

Because suitable single crystals of all systems of interest are not available, powder diffraction [24] has gained a new prominence in the study of the structure of zeolite/inclusion complexes. This allows the study of many molecular sieves which have

not been synthesized as single crystals. Further, the processes of dehydration and loading of the materials to be included can cause a decrease in crystal quality, making single crystal studies difficult to perform. Powder diffraction also has certain inherent advantages, including the comparative ease with which the molecular sieve can be loaded and handled.

Recent investigations of the structures of zeolite/inclusion complexes have benefited from the availability of dedicated synchrotron radiation sources, coupled with the design of flexible powder diffractometers at these facilities [6,16]. The advantages for the study of inclusion complexes are: high brightness, high peak to background discrimination and routine cooling capabilities to 20 K using Displex® refrigerators. Often molecules included into zeolitic materials disorder above a "freezing point"; data collected at low temperatures give the best chance of locating these species. Other improvements include the design and construction of readily interchangeable beamline-optics to optimize resolution to the problem at hand and more sensitive energy discriminating detectors, such as the position sensitive detector (PSD) recently described by Smith [25]. Provided some resolution can be sacrificed, the PSD is a powerful tool for the study of the zeolite/inclusion complex as a function of temperature or loading.

Most inclusion complexes involve some degree of disorder, either static or dynamic; in this case the powder diffraction experiment suffers an inevitable loss of information. The supplementing of diffraction data with information from NMR, molecular modeling, and other spectroscopic techniques is important in this work.

1.1.3 *EXAFS*

Diffraction techniques are most suited to structural studies of ordered materials. If the occluded species bind to a variety of sites on the walls of the zeolitic cavity, a more local probe is often appropriate. Extended X-ray absorption spectroscopy (EXAFS) is a popular technique for exploring the structure of occluded species in zeolites and has been used to postulate the geometry of these species and their relationship to the host framework. The ability of the EXAFS to yield local structural information has been reviewed elsewhere [26]. Essentially, the amplitude and frequency of oscillations, observed on the high energy side of the X-ray absorption edge for a particular element, are a function of the local environment for that element. By taking the Fourier transform of these oscillations, one obtains a radial distribution function. Refinement of parameters to best fit the observed oscillations for each shell of neighbors surrounding the absorber atom yields distances, coordination numbers, and displacement parameters. Prior knowledge of composition and possible geometries can be useful in translating this information into a credible model. For example, selenium exists in a number of allotropes, a helical chain form, and a number of ring structures. The allotrope stabilized in a variety of zeolitic hosts was shown to depend upon the geometry of the pore structure [27]. The EXAFS results, when combined with observations using optical absorption spectroscopy and NMR, showed the local environments for Se are consistent with the

helical form of this element when it is constrained in zeolites containing 1-D channels [27] (see Chapter 10 in this volume).

More recent examples of the use of EXAFS, in combination with a battery of complementary techniques, are reported by Ozin and co-workers [28 and references therein]. The systems of interest in these studies are stabilized semiconductor nanoclusters which have been induced to grow topotactically within the pores of selected zeolites. Disorder and partial occupancy of the available pore spaces required the interpretation of data, from a variety of sources, to deduce the nature of the semiconductor nanoclusters and their relationship to the host framework. Some of the techniques employed included reflectance spectroscopy, luminescence, elemental analysis, Rietveld refinement, as well as, EXAFS.

1.1.4 *Neutron Scattering*

Neutron scattering is the tool of choice when the positions of hydrogen atoms are of importance [17]. Recently the self-assembly of species in aluminosilicate gels impregnated with Pr_4N^+ ions was studied using small angle neutron scattering [29]. The scattering length densities of the gel particles and their texture were determined by using contrast variation methods [7]. Gels formulated with Pr_4N^+ template molecules promptly transform into an amorphous "embryonic" structure, and crystallization to zeolite ZSM-5 ensues via a solid hydrogel transformation mechanism. Gels formulated from colloidal silica without template show different scattering behavior from which a liquid-phase transport mechanism was inferred. Along with neutron spectroscopic studies of molecules trapped in zeolites using energy-loss spectroscopy, such investigations offer much promise for characterizing the interactions of absorbed species in microporous materials [7,29,30].

In this chapter, two systems studied using synchrotron X-ray powder diffraction are described. In both cases, the strengths of diffraction for determining site occupation, position and orientation are emphasized. In both studies, the importance of complementary analytical and spectroscopic techniques, along with insights provided by theoretical calculations and molecular modeling, are emphasized.

2. Xenon in Zeolite Rho

Distortions of the framework along with the type and number of adsorption sites, can affect the performance of microporous catalysts. Because the effects of physical and chemical changes on the framework of aluminosilicate RHO (Figure 1) are large [31-51] and the number of adsorption sites is apparently limited [52-56], it is an excellent model system for studying the interactions between zeolite frameworks and absorbed species.

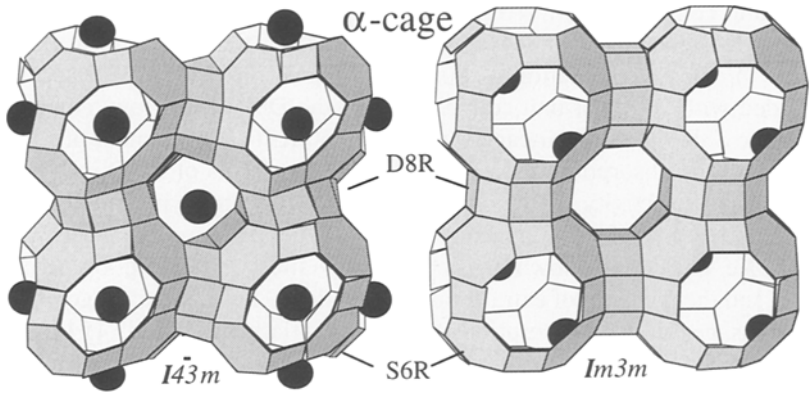

Figure 1. Representation of the acentric (left) and centric forms of zeolite rho. The acentric form is favored at low temperature, with exchange of small non-polarizable cations, and upon dehydration [39]. Upon heating, many divalent ion-exchanged forms undergo cation relocation. In the case represented here, Cd^{2+} moves from the center of the double 8-ring (D8R) to the wall of the α-cage near the single 6-ring (S6R) site.

Some of the most intriguing changes in RHO occur upon heating; one of these involves cation relocation [49]. Movement of exchangeable cations upon dehydration is a response to a loss of the H_2O ligand and a consequent need to satisfy coordination requirements [57-61]. In RHO, this movement can be dramatic [49,50] and affords an opportunity to study the interaction of absorbed species with mobile, exchangeable cations.

2.1 XENON IN H-RHO

As a prelude to studying the absorption and controlled release of Xe in the "trap-door" system Cd-rho described below, we decided to test the sensitivity with which we could locate Xe in H-rho. Diffraction studies of RHO [44-48] indicate it can adopt either a high or lower symmetry structure (Figure 1) depending on the conditions of treatment [36], hydration state, and extra-framework cations exchanged into the structure [37]. This structural change is accompanied by an elliptical distortion of the D8R pore opening (Figure 1), the degree of which is dependent on the unit cell parameters [48], and the nature of the framework cations [51]. A number of studies have examined the

relationship between the location of Xe in zeolite rho and such parameters as the number of Xe per unit cell, the temperature, and the degree of ion-exchange.

Working with a sample of RHO containing about 6 Xe per unit cell, or one for each D8R in the unit cell (Figure 1), Wright et al. [55] found Xe adsorbs at the center of the D8R-site at 5 K. When the sample was warmed to 245 K, the Xe was located at the S8R site (Figure 1). In an elaboration of this result, Gameson et al. [62] found that for a sample loaded with 2 Xe per unit cell, Xe prefers the D8R-site at low temperature and migrates to the S8R site on the α-cage wall above 160 K [62]. A number of studies have concentrated on the absorption of Xe in ion-exchanged forms of RHO in an attempt to clarify its unusual selectivity for the production of dimethylamine in comparison to other 8-ring zeolites [63,64]. In studies using NMR and temperature dependent absorption [54,56,65], Xe has been shown to occupy two sites depending on temperature, Xe-loading, and the presence of extra-framework cations. For ion-exchange of more than 2.67 Cs atoms per unit cell, sorption was "substantially inhibited" [54]. In recent theoretical studies [52,53], the occupancy by Xe of a second site in the α-cage, near the single six-ring (S6R, Figure 1), has been predicted to occur after the 8R-sites have been fully occupied. One intriguing possibility raised by this work is the existence of ordered Xe-clusters at very high loadings [53].

To test the capabilities of the diffraction experiment to locate Xe in zeolite H-rho, we chose a series of samples with an accurate chemical analysis and with well-determined absorption characteristics [54,56]. For this purpose, it was imperative that any residual Cs^+, which is extremely difficult to remove completely by ion-exchange [54], be accounted for; Cs^+ and Xe, since they are isoelectronic, are indistinguishable in the X-ray experiment. Xe was loaded into approximately 0.3 g batches of H-rho. The chemical analysis obtained for this sample, based on inductively coupled plasma spectroscopy [54], showed it to have the unit cell formula $H_{10.77}Na_{0.48}Cs_{0.75}$-$Al_{12}Si_{36}O_{96}$; the H^+ are added to the formula to charge balance the analyzed value for Al, which is presumed to occupy only framework positions. Samples were loaded at 1, 50, 100, 200 and 400 torr in glass capillaries 1 mm in diameter. The isotherm for Xe absorption in this system has been determined at 300 K allowing the calculation of the number of Xe expected to sorb per unit cell (Figure 2). Three sites can host Xe: the D8R-site at the center of the octagonal prism, the S8R near the surface of the α-cage and about 1.5 Å from the D8R-site, and the S6R on the surface of the α-cage (Figure 1).

X-Ray powder diffraction data for Xe-loaded H-rho were collected at 300 K at the National Synchrotron Light Source (NSLS) beamline X-7A. This facility can be configured to operate in a variety of diffraction geometries by replacing optic elements and detectors [6,16]. For this experiment, a positron sensitive detector designed and built at the Brookhaven National Laboratory (BNL) [25] was used. The unique features of this detector design have been described by Smith [25] and include exceptional angular resolution and peak-to-background discrimination; the ability to discriminate against fluorescent background is particularly effective in obtaining data suitable for structural refinement [66].

The data were analyzed using the Rietveld Technique [66] implemented in the GSAS (Generalized Structure Analysis System) suite of programs [67]. The diffraction data could be indexed on the basis of a body centered cubic cell approximately 15 Å on edge, suggestive of the $Im\bar{3}m$ symmetry structure (Figure 1) of RHO [37,48,51].

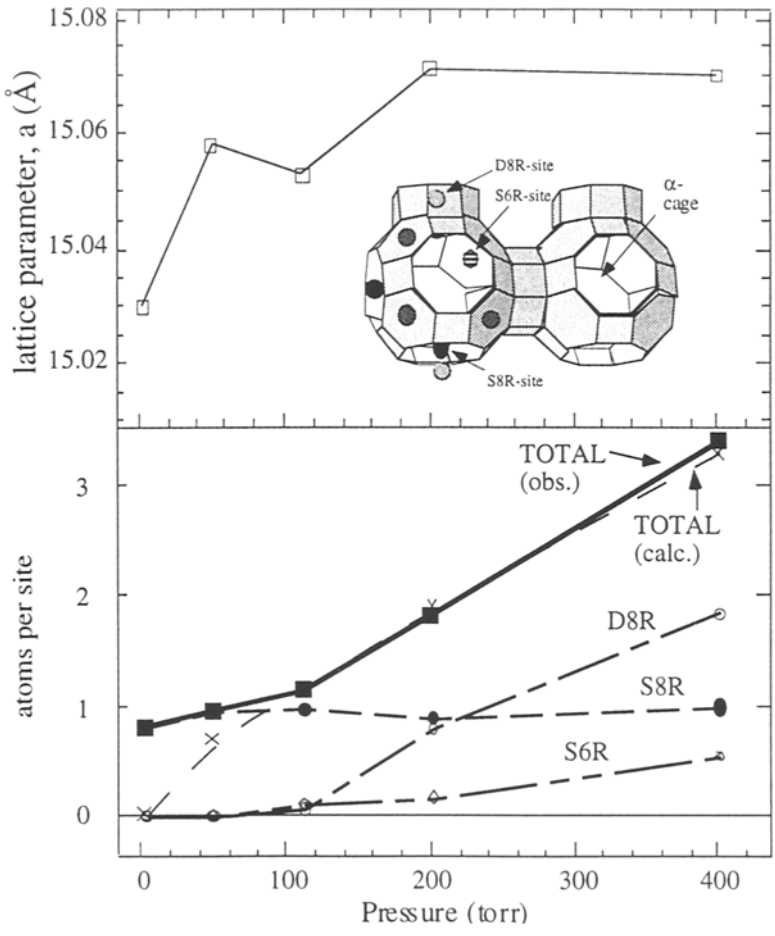

Figure 2. Variation in the lattice parameter (upper) and a summary of the results of site occupancy refinements for H-rho (0.75 Cs) loaded with Xe (lower) at the pressures indicated (see Table 1). Up to 200 torr, the 8-ring site on the wall of the α-cage is preferred over the site in the center of the octagonal prism (Figure 1). Above this loading, while the occupancy of the former site remains constant, the Xe loads preferentially into the D8R site in the octagonal prism. A third site, the S6R on the wall of the α-cage, is occupied after a loading pressure of 100 torr and increases in occupancy as the pressure increases.

The powder diffraction pattern for the H-rho loaded at 1 torr clearly contained contributions from two cubic unit cells with different cell parameters (Figure 3); these were 15.033(1) and 14.947(1) Å. This sample afforded an unexpected opportunity to test the accuracy of the chemical analysis, and to locate the residual Cs found in the chemical analysis of the H-rho. The model best-fitting the RHO with the smaller unit cell was found to contain scattering from only the D8R-site (Figure 1). This scattering was best modeled with 0.15(1) Cs atoms in the 6-fold site at ($^1/_2$,0,0) giving a total of 0.90(6) Cs per unit cell (close to the chemically analyzed value of 0.75 Cs atoms per unit cell). Given that these refinements were carried out using fixed values of U = 0.06 Å^2 for the thermal parameters of the extra-framework material, there is good agreement between chemically analyzed Cs and that found in the diffraction experiment. No scattering was found near the 6R-site (Figure 1) at *x,x,x* with *x* = 0.37. For the RHO with the larger cell parameter, scattering was found at the D8R-site, corresponding to 0.75 Cs, as well as at the S8R-site at *x*,0,0 with *x* = 0.39 (Table 1). This extra scattering was presumed to arise from Xe absorption. For refinement of the other samples, the D8R-site was presumed to contain a fixed occupancy of 0.75 Cs, consistent with the chemical analysis.

Previously published structural data [31,47,68] were used as a starting point for development of the models consistent with the observed data. Using the 400 torr data set, three sites were identified for the adsorption of Xe from inspection of Fourier difference maps [67] and subsequent refinement of occupation factors (Table 1). These sites were at the center of the octagonal prism (D8R-site) and on the wall of the α-cage at the S6R- and the S8R-sites (Figures 1 and 2). These sites have oxygen nearest neighbors at the following distances: for the S8R-site, four at 3.281(6) Å; for the D8R-site, eight at 3.754(7) Å; and for the S6R-site, three at 3.85(8) Å The refinements for the remaining samples commenced by refining the site occupation factors for these three sites (Figure 2); the 0.75 Cs was presumed to occupy the D8R-site throughout. The framework atoms were initially fixed at positions predicted from distance least squares (DLS) modeling [48,67,69] based upon framework distances and the lattice parameter for the particular sample (Figure 2). All parameters, except the thermal parameters for the extra-framework sites, were varied in the final refinements.

The number of atoms of Xe occupying each site is summarized in Figure 2. At the lowest loadings (<100 torr), all adsorbed Xe visible to X-rays occupy the S8R-site on the wall of the α-cage. Above this pressure, Xe begins to occupy the D8R-site while maintaining an almost constant occupancy of the S8R-site; it appears that, *at 300 K*, the S8R-site saturates quickly. Above 200 torr at 300 K, the D8R site is preferred site for adsorption by a ratio of 2:1, compared with the S8R at 400 torr. The occupancy of the second site on the α-cage, the S6R (Figure 1), also increases above 100 torr. Essentially all the Xe, predicted to be absorbed from previously published isotherms [54], was found in the diffraction experiment. The exception is the non-equilibrated sample loaded at 1 torr. This sample contains two phases, one with and one without Xe; equilibration would distribute the Xe into a larger quantity of H-rho (Figure 2) and bring the observed loading closer to the curve calculated from the measured isotherms [54].

Table 1. Refined* positional and occupation parameters for Xe in H-rho.

Pressure	1 torr¶	50 torr	110 torr	200 torr	400 torr
x_T†	0.1016(1)	0.1011(1)	0.1008(1)	0.1013(1)	0.1019(2)
$x_{O(1)}$†	0.1673(1)	0.1682(2)	0.1685(2)	0.1680(2)	0.16736(2)
$z_{O(1)}$†	0.3741(4)	0.3762(4)	0.3770(4)	0.3758(4)	0.3739(5)
$y_{O(2)}$†	0.2187(4)	0.2169(4)	0.2159(4)	0.2177(4)	0.2198(5)
$z_{O(2)}$†	0.3772(2)	0.3788(2)	0.3791(3)	0.3789(2)	0.3780(2)
occ Xe(1)	-	-	-	0.135(4)	0.310(7)
$z_{Xe(2)}$†	0.390(3)	0.375(3)	0.400(2)	0.380(3)	0.389(4)
*occ*Xe(2)	0.080(4)	0.072(3)	0.085(3)	0.072(3)	0.085(4)
$x_{Xe(3)}$†	-	-	0.375(9)	0.373(4)	0.376(3)
*occ*Xe(3)	-	-	0.007(3)	0.020(4)	0.036(6)

* in all refinement chemically analyzed $Cs_{0.75}$ fixed at position 6*b*, $(0,0,1/2)$ with occupancy 0.125 .

† space group $Im\bar{3}m$, T at site 48*i* ($1/4$, *y*, $1/2$-*y*), randomly occupied by $Al_{12}Si_{36}$; O(1) at site 48*k*, (*x*,*x*,*z*); O(2) at site 48*j*, (0,*y*,*z*); Xe(1) at site 6*b*, $(0,0,1/2)$; Xe(2) at site 12e, (0,0,*x*); Xe(3) at site 16f, (*x*,*x*,*x*).

¶ nominal pressure, since Xe-containing phase occurs in the same sample as unloaded H-rho ($Cs_{0.75}$; see Figure 3); the refined phase fractions [67] for the unloaded and loaded phases are 0.70(1) and 0.30(1), respectively; positional and occupancy parameters for the Xe-loaded phase reported here.

The behavior of Xe above 200 torr (Figure 2) is in agreement with previous studies at fixed loading but at lower temperatures [55,62]. It is also consistent with recent theoretical work [52]. At 300 K and at loadings above 200 torr, Xe prefers the D8R site (Figures 1 and 2). However, at 300 K, the S8R-site is occupied by a constant amount of Xe, regardless of loading pressure, up to the maximum studied here, 400 torr. At a loading below 200 torr, the preference for the S8R-site is at odds with predictions based upon theory [52].

This preliminary study showed we could locate small quantities of Xe and discern small differences in occupancy between the D8R-sites and those on the walls of the α-cage. It also showed that at 300 K essentially all the Xe is localized, on the time scale of the X-ray experiment. This confirms the high interaction energy with the aluminosilicate framework proposed by Tsaio et al. [54].

2.2 XENON IN Cd-RHO

The powder X-ray diffraction patterns of some divalent cation-exchanged RHO display abrupt changes at high temperature [37]. Structural studies [49] reveal that these "transitions" are not associated with water loss, but rather accompany relocation of the cation from the D8R-site. For example, the unit cells for the Ca^{2+}-, Sr^{2+}-, and Ba^{2+}-exchanged materials underwent a rapid decrease in volume associated with movement

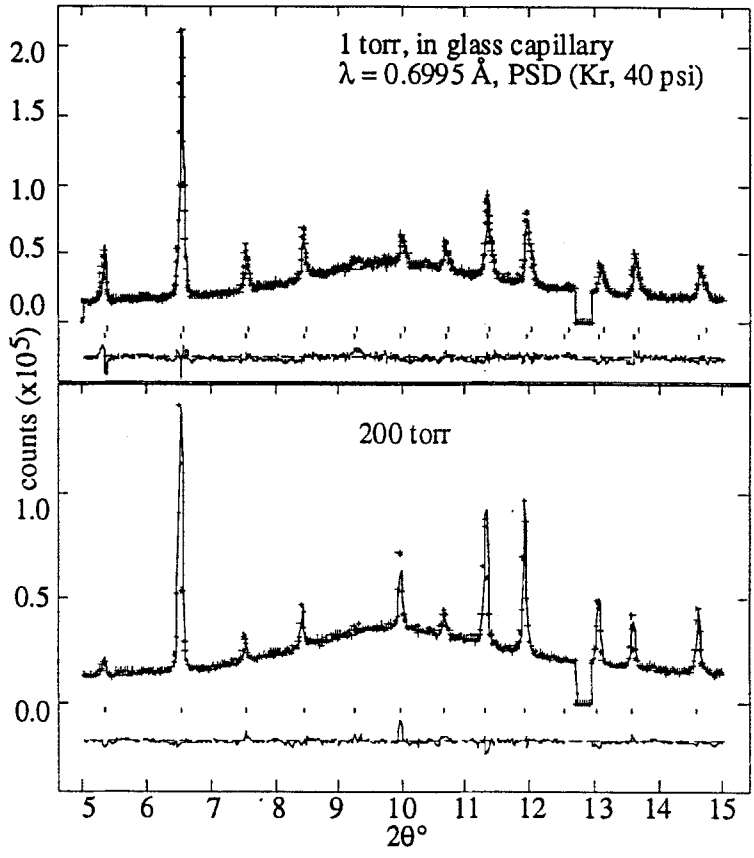

Figure 3. Comparison of the fit between observed (crosses) and calculated (continuous line) profiles [67] for H-rho loaded with Xe at 1 (top) and 200 torr. The difference between the observed and calculated profiles is plotted beneath each on the same scale. Two distinct phases are present in the sample loaded at 1 torr; the vertical dashes indicating the 2θ–positions of the Bragg reflections for each phase. The broad hump in the diffraction pattern centered at 10°, arises from scattering from the glass capillary containing the sample.

(Figure 1) of the cations within the 8R-sites [34,35,49]. However, in the case of the Cd^{2+}-exchanged RHO the unit cell parameter *increased* abruptly from 14.5 Å to 15.0 Å. A complete structure analysis using data collected in situ at temperatures above and below the transition [49,50] revealed the consequences of this change in cell volume; the Cd^{2+} ion undergoes relocation from the 8R-site in the octagonal prism to the S6R-site on the wall of the α-cage (Figure 1). This relocation is the largest in a zeolite (some 5Å) and

involves the opening of access to the α-cage above the transition temperature of 400° C. Upon cooling to 300° C, Cd^{2+} moves back to the 8R, thereby restricting access to the α-cage. More recently, we have also observed this behavior in Zn-exchanged RHO and are pursuing structural studies on this material as well.

This property suggested Cd^{2+} could behave as an ionic trap door. While the trap door is open, above the transition to the $Im\bar{3}m$ form of RHO (Figure 1), sorption to the interior of the zeolite by molecules small enough to negotiate the D8R is permitted. Following sorption above 400° C, cooling below the transition temperature traps the sorbed guest; the Cd^{2+} moves back into the 8R as the framework distorts to the lower volume $I\bar{4}3m$ form of RHO (Figure 1). Provided the Cd^{2+} trap door remains in place, the sorbed guests, reactants, or products should be retained in the α-cage (Figure 1). Previously determined isotherms for Cs-RHO have shown that, for more than 2.67 Cs per unit cell, sorption is "substantially inhibited" [54], suggesting less than complete Cd^{2+}-exchange was required to test the philosophy outlined above.

2.2.1 *Static Studies*

The ability to trap and release Xe was demonstrated by thermogravimetric/mass spectral analysis (TG/MS) and ^{129}Xe-NMR [70]. A sample of Cd,NH_4-rho, $[Cd_{3.3}(NH_4)_{5.42}Na_{0.03}Cs_{0.25}]Al_{12}Si_{36}O_{96}$ (NH_4^+ content is assumed for charge balance), was prepared by conventional NH_4^+-exchange followed by Cd^{2+}-exchange of Na,Cs-rho [71,72]. The sample of Cd,NH_4-rho was out-gassed for 10 days at 400° C under 10^{-5} torr. It was then placed in a bomb, charged with 200 psi of Xe, and heated to 350° C for 2 hours. After cooling to room temperature, the pressure was decreased to 25 psi and the sample was transferred to a dry-box. Here, samples for NMR, TG/MS and powder diffraction were prepared for analysis.

In the TG/MS results, given in Figure 4, the event at 340° C was attributed solely to desorption of xenon (m/z=129). Ion peaks corresponding to all of the isotopes of xenon as well as the +2 ions were observed. The appearance of xenon at this temperature correlates well with the in situ X-ray powder diffraction results [49,50]. These show the Cd is relocated away from the 8-ring opening allowing the entrapped Xe to egress from the α-cage above this temperature (Figure 4). The weight loss of 5.7% associated with this escape corresponds to a loading of approximately 0.85 Xe/α-cage or 1.7 Xe/unit cell. This corresponds to approximately half of the Xe found in the diffraction experiment described below; considering the amount of water sorbed, significant amounts of Xe may have been lost during the transfer to the TG apparatus. Diffraction experiments which follow the desorption of Xe in real time are described below. They confirm the loss of about half of the Xe within 1 hr of the sample being exposed to the atmosphere.

Additional events are observed at approximately 100° C and 520° C, with weight losses of 9.8 and 0.93%, respectively. The ion chromatograms associated with water (m/z=18, 17) show the low temperature event, along with small events at about 290° C and 390° C, are associated with the desorption of water, most likely sorbed during transfer from the

dry box to the TG apparatus. In addition, the event at 520° C appears to be associated with loss of ammonia (m/z=17). Apparently, the out-gassing at 400° C was not sufficient to completely deammoniate the Cd,NH_4-rho.

To compare the siting of Xe in this case with that found in the case of Xe loaded into H-rho described above, we carried out diffraction experiments at room temperature (300 K) and at 13 K. A sample from the batch of Cd/Xe-rho described above (Figure 4) was loaded into thin-walled glass capillaries in a dry box. Constraints imposed by the geometry of the Displex® low temperature unit at X-7A made the task of sealing these 0.7 mm OD x 20 mm capillaries a challenge. Several were surveyed at room temperature before one was deemed suitable for data collection at 13 K. The rapid survey was accomplished using a linear position sensitive detector designed and built at the BNL [25]. This gas proportional detector, when operated with X-rays near 40 keV and 40 psi of Kr gas, gives good resolution and high peak-to-background discrimination by gating on the Kr escape peak [25]. Samples, which had been improperly sealed, were found to give patterns which could be indexed on the basis of a 15 Å unit cell; this was indicative of the Cd-rho having hydrated and lost Xe. Some capillaries were found to have the dehydrated form intact. One of these was placed in the Displex® refrigeration unit and a full data set was collected at 300 K. The sample was then cooled to 13 K.

The 13 K data were collected in high resolution mode [6,16]. The positional parameters for the TO_4 framework (T = Al/Si) were fixed, in accordance with the lattice parameters and the results of DLS modeling [48,67], as were the isotropic thermal parameters.

Unconstrained refinement of the occupation factor for a dummy oxygen atom placed in the D8R, S8R, and two S6R-sites (Figure 1, Tables 1 and 2) suggested these sites are occupied. After assigning the scattering factor for Cd to those sites with occupancies greater than one, the occupation factors were once more refined. From this and from the results of calculated Fourier Difference maps, six atoms were located in the 8R-octagonal prism. The scattering is equally distributed between two sites, close to the center of the D8R and offset from the center of the S8R (Figure 5, Table 2). This implies that 2.7 Xe, along with the 3.3 Cd found in the chemical analysis, occupy this structural unit. In order to determine possible site distributions, a series of models was tested. In one such trial, the occupancy of the S8R- and D8R-sites were refined without constraints; the sites were assigned the scattering factors of Cd and Xe, respectively. This resulted in a calculated formula of $Cd_{3.44(2)}Xe_{2.78(4)}$ for the octagonal prism when all the Cd is located in the S8R and all the Xe is in the D8R-site. This is close to the expected total of six, for the six octagonal prisms per unit cell, and close to the total Cd found in the chemical analysis. Although the large contributions to the scattering from both Xe and Cd aid in their location in the X-ray experiment, their closely matched scattering factors makes distinguishing between them difficult. Indeed, refinements of the fully hydrated/ completely Xe-desorbed sample described in the next section, suggests that Cd is partially disordered over the two sites, but with a preference for the S8R-position. On the basis of a model in which all octagonal prisms were occupied with either Cd at the S8R-site or Xe at the D8R-site, a complete refinement was obtained based upon the 13 K data

set (Table 2). The assignment of the Xe and Cd to the sites near (x,0,0) with $x \approx 0.5$ and $x \approx 0.35$ respectively, was on the basis of an ordered arrangement of Xe and Cd within the octagonal prism. When the positions of the Cd and Xe were reversed from those given in Table 1, the refinement led to a composition $Cd_{2.5}Xe_{3.6}$, a worse match to the observed chemistry ($Cd_{3.3}$) than that found in the final refinement (Table 1) of $Cd_{3.8}$ for the 13 K data set.

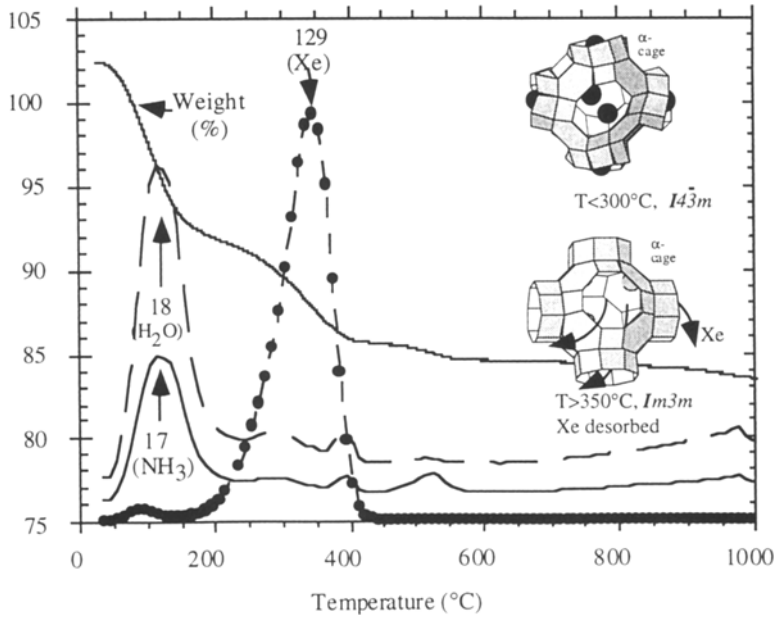

Figure 4. TG/MS plots for Xe-loaded Cd,NH_4-rho as a function of temperature. The weight loss refers to the left hand scale while the relative intensity of the desorption peaks is referred to the scale to the right.

The possibility that Cd and Xe are partially disordered over these two sites can not be ruled out based on these results. A neutron diffraction experiment would also probably fail to resolve the two site chemistries. Not only is Cd highly absorbing to neutrons, but the Cd and Xe scattering lengths differ by only 2%; they differ by 12% at $\sin\theta/\lambda = 0$ for X-radiation. This problem could be resolved using anomalous scattering techniques [16]. Because of the energies of the edges involved (≈30 keV), this experiment is probably best carried out on the third generation synchrotron sources currently being prepared for use.

In addition to the two sites in the 8-rings, two other sites were found to be occupied. One, which was at *(x,x,x)* with $x \approx 0.15$, amounted to the equivalent of 1.4 Xe per unit cell, while the other site, at *(x,x,x)* with $x \approx 0.35$, was found to be occupied by 0.1 equivalent atoms of Xe per unit cell. This later site, clearly less preferred by Xe, may be residual H_2O not removed during the dehydration process. For the final refinements, utilizing the 13 K and 300 K data sets, Cd was located at site 24g (*x,y,y;* $x \approx 0.35$, $y \approx -0.06$) Xe(1) at site 12e (*x,0,0;* $x \approx 0.54$), Xe(2) at 8d (*x,x,x;* $x \approx 0.14$) and O(H_2O) at 8d (*x,x,x;* $x \approx 0.31$). The total content of the octagonal prisms was constrained to equal six. The results for the final refinements of both the 13 K and 300 K data are given in Tables 1 and 2.

Table 2. Positional, thermal and occupation factors for Cd/Xe-RHO* at 13 (top) and 300 K.

Atom	site/occ.	*x*	*y*	*z*
T(1)†	48*h*/1.0	0.2673(2)	0.1183(2)	0.4170(3)
		0.2676(2)	0.1180(2)	0.4174(2)
O(1)	24*g*/1.0	0.2121(5)	0.2121(5)	0.3951(7)
		0.2077(3)	0.2077(3)	0.3926(5)
O(2)	24*g*/1.0	0.1341(3)	0.1341(3)	0.6194(5)
		0.1349(3)	0.1349(3)	0.6228(4)
O(3)	48*h*/1.0	0.0263(3)	0.2128(3)	0.3864(4)
		0.0266(2)	0.2136(3)	0.3857(3)
Cd(1)¶	24*g*/0.158(1)	0.3487(8)	-0.0569(5)	-0.0569(5)
	24*g*/0.163(1)	0.3365(9)	-0.0568(5)	-0.0568(5)
Xe(1)¶	12*e*/0.184(3)	0.541(1)	0	0
	12*e*/0.174(3)	0.540(2)	0	0
Xe(2)	8*c*/0.173(4)	0.1460(7)	0.1460(7)	0.1460(7)
	8*c*/0.158(4)	0.144(1)	0.144(1)	0.144(1)
O(H_2O)	8*c*/0.18(4)	0.318(5)	0.318(5)	0.318(5)
	8*c*/0.21(4)	0.304(5)	0.304(5)	0.304(5)

* RHO framework, $I\bar{4}3m$, a=14.6886(6) and 14.712(1) Å, for 13 K and 300 K data, respectively. Refinement statistics (%) [67] with values for 300 K data in parentheses: R_{wp} = 8.00(6.72), R_p = 6.65(5.23), R_{Bragg} = 5.61(5.23), χ^2 = 0.75(0.70). Isotropic thermal parameters for all extra-framework atoms fixed at U = 0.06 $Å^2$; those for the framework (T and O-sites) constrained to be equal and refined to U = 0.007(1) at 13 K and U = 0.002(1) $Å^2$ at 300 K.

† Scattering adjusted to match framework cation composition [$Al_{12}Si_{36}$] from chemical analysis.

¶ total occupancy constrained to 6 per unit cell.

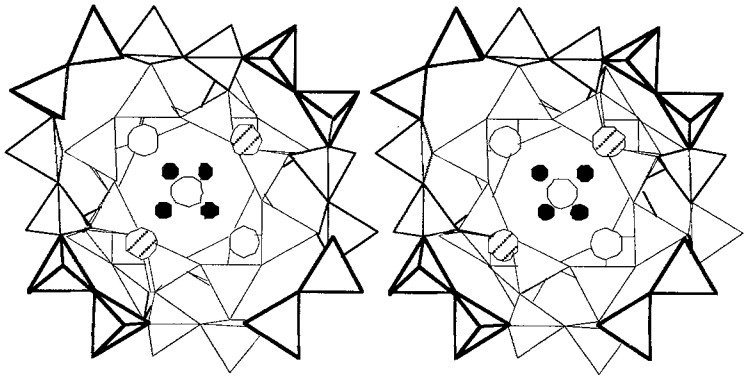

Figure 5. Stereo representation of the interior of the α-cage showing the positions of Xe (blank circles), Cd (black), and either water, ammonia or low occupancy Xe site (striped) marked O(H_2O) in Tables 2 and 3. The Xe at the center of the 8-ring and at the S6R-site are marked Xe(1) and Xe(2), respectively, in Tables 1 and 2. Interatomic distances are given in Table 3.

The preference of Xe for the 8R site is consistent with the previous theoretical work on H-rho. However, in that work, account was not taken of cases in which the 8R-site was partially occupied by a tightly-bound cation. In the present study, this situation leads to occupancy of one the S6R-site on the wall of the α-cage (Figure 5, Table 2). The occupancy of only one of these sites may be indicative of a Cd-Xe or Xe-Xe interaction since this is possible only from the Xe(2)-site (Figure 5).

2.2.2 Real-Time Studies of Xe Desorption

During the dismounting of one of the samples used to study Xe in Cd-exchanged zeolite rho, the capillary in which it was contained broke. Changes were observed to occur as data in the PSD were being collected. This afforded an unexpected opportunity to study the desorption of Xe from the sample in real time.

The PSD detector being used for this work [25] is capable of collecting data in less than 10 minutes; these data would be to a resolution of 1 Å and suitable for Rietveld [66] refinement. Unfortunately, a certain lack of urgency on our part limited the time resolution to about 40 minutes. During this time period, the diffraction patterns were evolving with the lattice parameters of phases changing and new phases appearing (Figure 7). The implications of this type of study are obvious, however. Real-time monitoring of sorption/desorption and of ion-exchange processes is feasible. All that is required is a means of placing materials under controlled atmosphere, temperatures, and

pressure. In the future, more intense X-ray beams, such as those proposed for the third generation synchrotron sources currently under construction, will greatly aid these investigations. The more intense beams will also require redesign of data acquisition and analysis systems to cope with the volumes of data produced in these types of studies.

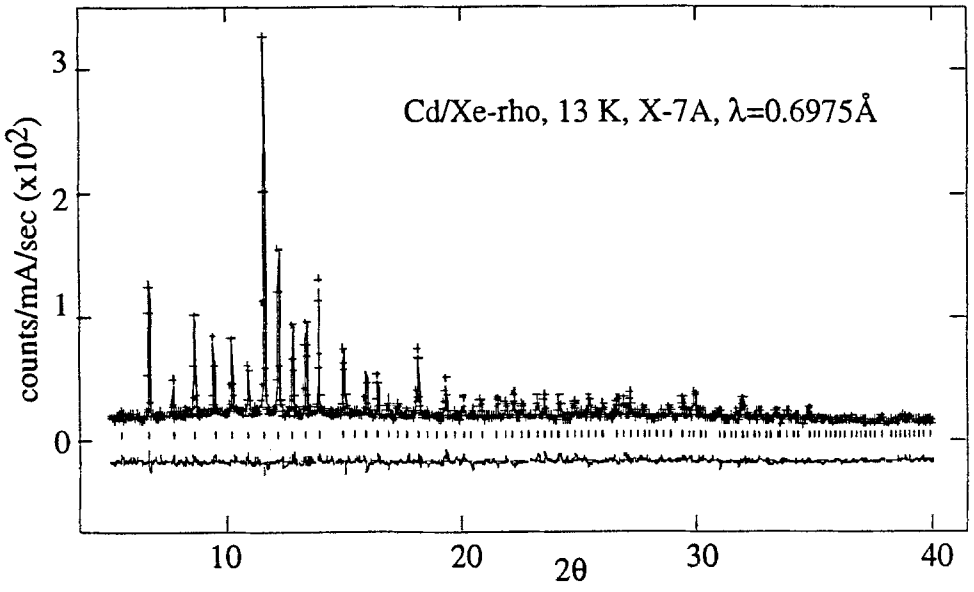

Figure 6. The X-ray diffraction data for Cd,NH_4-rho loaded with Xe (referred to as Cd,Xe-rho) at 13 K. Points shown by (+) represent observed data. The continuous lines through the sets of points are the data calculated from the model given in Table 2. The set of tic marks below the data indicate the positions of the allowed reflections. The lower curve in each panel represents the difference between observed and calculated profiles.

Since there are distinct phases contributing to the powder diffraction patterns, and not just one or two with continuously varying lattice parameters, this implies a competition between sites as Xe is desorbed and H_2O is sorbed. This is similar to the situation observed in Cd,NH_4-rho at high temperature where the competition is between occupancy of the 8R- and 6R-sites as the framework transforms from $I\bar{4}3m$ to $Im\bar{3}m$ symmetry at 350° C [49,50,70].

For the structural refinements, the framework atomic positions were initially fixed at values obtained from DLS modeling. Following refinement of site occupation factors and in the final stages of model refinement, soft constraints on the interatomic distances between atoms in the aluminosilicate framework were introduced to supplement the diffraction data and allow adjustment of all positional parameters.

Table 3. Selected interatomic distances (Å) and angles (°) for Xe in Cd,NH_4-rho at 13 and 300 K.

atoms	13 K	300 K	atoms	13 K	300 K
T(1)-O(1)	1.632(1)	1.628(1)	O(1)-Si(1)-O(2)	110.0(3)	109.6(1)
T(1)-O(2)	1.630(1)	1.629(1)	O(1)-Si(1)-O(3)	113.6(6)	109.9(2)
T(1)-O(3)	1.634(1)	1.630(1)	O(1)-Si(1)-O(3)	108.6(6)	109.9(2)
T(1)-O(3)	1.634(1)	1.631(1)	O(2)-Si(1)-O(3)	108.5(3)	109.2(2)
			O(2)-Si(1)-O(3)	107.1(3)	108.5(2)
Cd(1)-O(2) x2	3.063(8)	3.104(7)	O(3)-Si(1)-O(3)	108.9(3)	109.7(2)
Cd(1)-O(3) x2	2.398(6)	2.458(7)	Si(1)-O(1)-Si(1)	143.3(5)	145.8(3)
Cd(1)-Cd(1)	2.36(2)	2.36(2)	Si(1)-O(2)-Si(1)	144.8(5)	146.1(4)
Cd(1)-Xe(1)	3.07(2)	3.21(3)	Si(1)-O(3)-Si(1)	137.4(3)	137.7(3)
Cd(1)-Xe(1)	2.00(1)	2.17(2)			
Cd(1)-Xe(2)	3.50(1)	3.36(1)	Xe(1)-O(2) x2	3.013(8)	3.06(1)
			Xe(1)-O(2) x2	3.65(1)	3.68(1)
Xe(2)-O(1) x3	3.91(2)	3.90(2)	Xe(1)-O(3) x4	3.88(1)	3.89(1)
Xe(2)-Cd(1) x3	3.50(1)	3.36(1)	Xe(1)-O(3) x4	3.323(8)	3.35(1)
O(H_2O)-O(1) x3	2.48(6)	2.39(5)	Xe(1)-Xe(1)	1.21(3)	1.16(5)

The occupation factors derived for four phases identified in this study are summarized in Table 4. Occupancies are given as numbers of atoms per unit cell. The scattering factors were arbitrarily assigned to conform to the distribution found in the study of the fully loaded materials (Tables 2 and 3). The fully hydrated centric form of Cd,NH_4-rho, designated D (Table 4, Figures 7 and 8) can be used as a baseline in proposing a scenario for the Xe-desorption process. It was presumed this phase represented the fully desorbed form and that any scattering found arose from either Cd or H_2O; scattering from N and O in NH_4^+ or H_2O were not distinguished. This assumption was reinforced by the closeness of the match between the amount of Cd found in the refinement of the phase D structure model, 2.8 Cd (Table 4), and that determined from the chemical analysis, 3.3 Cd. Another aspect of the refinement for phase D concerns the position of Cd in the hydrated material; Cd is found to prefer the S8R-site, but also to partially occupy the D8R-site. Indeed, the changes in the occupancy of these two sites from phase A' through D (Table 4, Figure 7) suggests that upon Xe loss and hydration there is considerable mobility of Cd.

Most of the Xe (40%) is lost within the first hour following exposure to the atmosphere and explains why only half the Xe expected is found in the TG/MS experiment (Figure 4). This causes a dilation in the unit cell as the sorbed gas is lost (Table 4). Following the initial loss of all Xe from the 8R site in phase A' (Table 4, Figure 7), a comparatively slow rearrangement and loss of Xe from the S6R occurs, possibly as a response to competition with sorbed H_2O. Phase B, for example, has about the same total Xe in the S6R as the sealed sample but equally distributed over the two available sites rather than

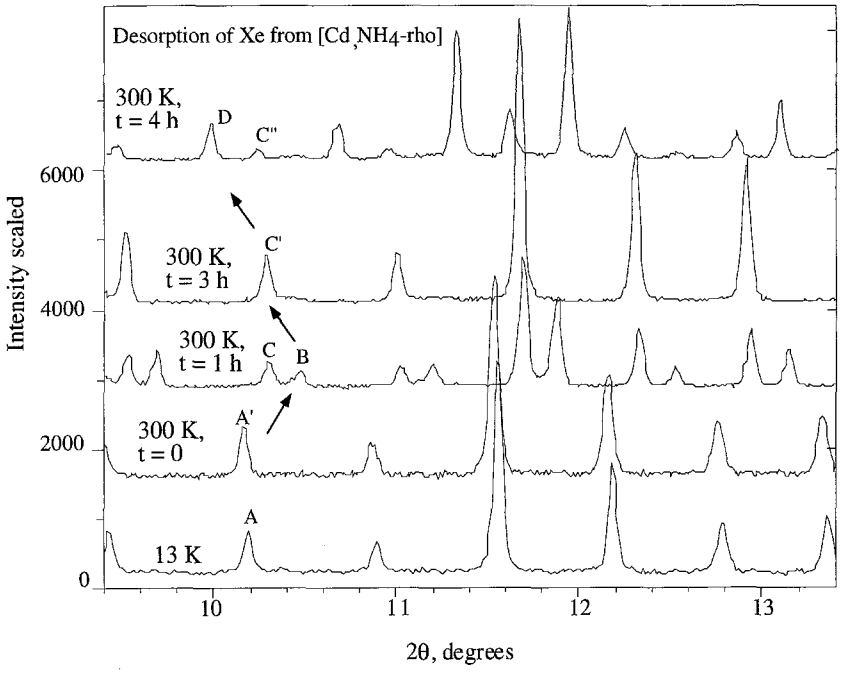

Figure 7. Stack-plot of representative diffraction patterns collected from Xe-loaded Cd,NH_4-rho. The times (t, in hours) refer to the start time for the particular pattern after the contents of the capillary had been exposed to the atmosphere.

concentrated on the site at (x,x,x); $x = 0.15$. The unit cell edge (Table 4) gradually increases as the sample hydrates and loses Xe.

Clearly, this type of transformation is worthy of further investigation using other cation/gas combinations in RHO, and possibly other zeolite systems. Structure analysis using the data collected here was complicated by the lack of time resolution obtained during data collection. The contributions from particular phases (Figures 7 and 8) are changing with time and the lattice parameters of those phases are also changing. This situation would be greatly improved by shorter data collection times and such studies are planned. The broader implications for this study are clear. Given a gas pressure cell, the technology now exists to collect and analyze X-ray data taken in real time on desorbing zeolites, and to obtain meaningful structural information from these data. This philosophy can easily be extended to studies of ion-exchange in real time as well.

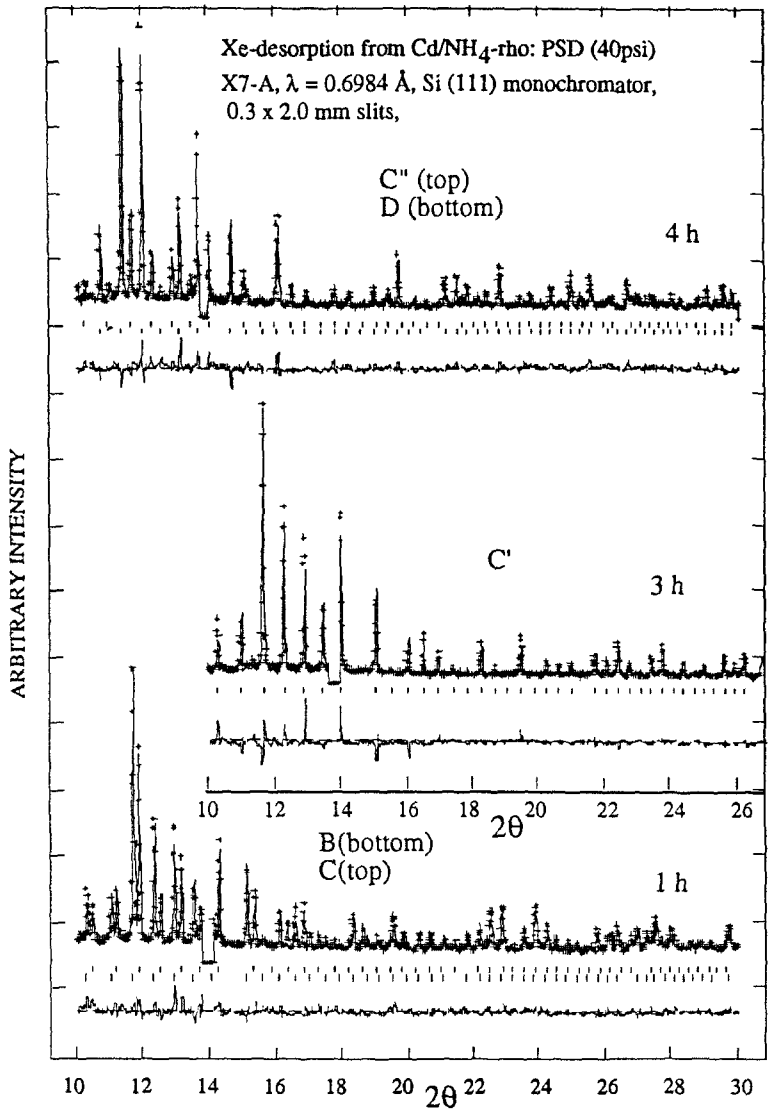

Figure 8. Observed (crosses) and calculated (continuous line) profiles for three samples of Xe desorbing from Cd,NH_4-rho. The difference curves are plotted below each pattern and tick marks refer to the Bragg positions of the diffraction maxima for the phases indicated here, in Figure 7 and Table 4.

Table 4. Results of site occupancy refinements* for the phases shown in Figures 7 and 8.

	sites			
phase/*a* (Å)	S8R† (Cd)	D8R (Xe)	S6R (Xe @*x*=0.15)	S6R (Xe@*x*=0.35)
A'/14.712(1)	3.91(2)	2.09(4)	1.26(4)	¶
B/14.332(1)	1.53(3)	0.57(2)	0.88(4)	0.72(4)
C/14.557(1)	1.44(3)	1.04(2)	1.03(6)	0.24(6)
C'/14.631(1)	0.48(3)	1.08(3)	0.72(4)	0.56(4)
C''/14.657(1)	1.2(2)	1.63(3)	0.90(6)	0.80(4)
D/15.033(2)	1.92(2)	0.84(2)	<·····$8H_2O$§·····>	

* During these refinements soft constraints were used to supplement the diffraction data; thermal parameters were fixed at U=0.02 and 0.06 Å^2 for framework and extra-framework sites, respectively.

† Scattering factor set to Cd or Xe based upon results of 300 K refinement of dehydrated and hydrated material which suggested the S8R is the preferred site for Cd.

¶ occupied by 1.7 H_2O or equivalent scattering material (NH_4^+ for example).

§ space group $Im\bar{3}m$, S6R-sites are equivalent.

3. Stilbene in ZSM-5

Recently, the shape selective properties of zeolitic materials have inspired organic chemists to use them as platforms for a variety of polymerization and photochemical reactions [73-78]. Some of these studies [77,78] involved the sorption of *trans*-stilbene ($C_6H_5C_2H_2C_6H_5$), and the stabilization of its thermally-activated radical cation, in Na-ZSM-5. We thought it worthwhile to investigate the effects of stilbene absorption on the framework geometry of ZSM-5 and to locate the molecule within the structure.

ZSM-5 is a high silica aluminosilicate molecular sieve with a unique pore geometry consisting of intersecting 10-ring channels (Figure 9). One of these, the "straight" channel, is parallel to the ***b***-axis and has a free diameter of approximately 5.5 Å [1]. The second is a slightly elliptical (5.5 x 5.1 Å), 10-ring sinusoidal channel parallel to ***a***, with a half-wave period equal to ***a***/2; or approximately 10 Å [1]. Using Van der Waals radii, the stilbene molecule is estimated to be about 11.5Å long, suggesting it may be difficult to fit this molecule into the sinusoidal channel without distorting it.

The complex framework of ZSM-5 ($\boldsymbol{a} \approx \boldsymbol{b} \approx 20$Å, $\boldsymbol{c} \approx 13.4$Å, $\boldsymbol{U} \approx 5360$ Å^3) displays a rich structural chemistry with variation in temperature, Si/Al-ratio, and sorbate loading [18,20,21,79-84]. The as-synthesized material, containing a template molecule such as tetrapropylammonium, is orthorhombic, ***Pnma*** [1]. It distorts to monoclinic ($\boldsymbol{P2_1/m}$) upon removal of the template and conversion to the H-form [18], which in turn exhibits a reversible phase transition at about 340 K. The orthorhombic form is stable above and the monoclinic form stable below this temperature. Further, the crystal symmetry is affected by the amount and type of sorbate [81] (Figure 10).

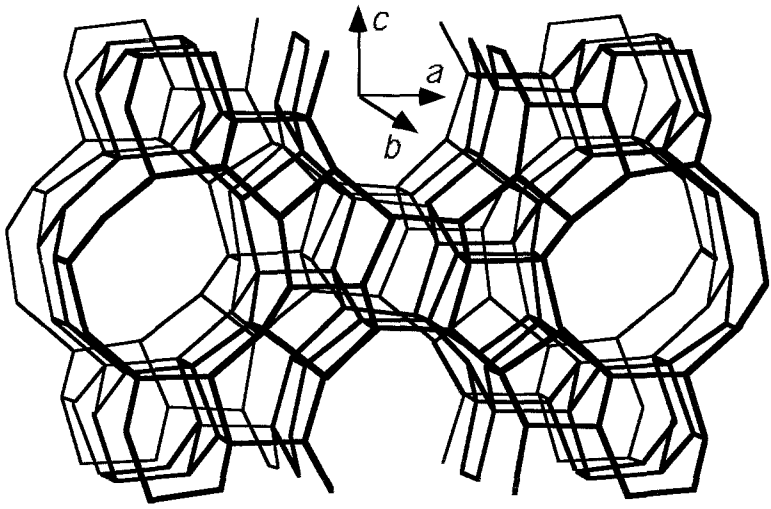

Figure 9. Structure of the ZSM-5 framework (***Pnma***) viewed along [*010*]. The straight 10-ring channels are parallel to the ***b***-axis while the direction of the sinusoidal 10-ring channel is parallel to the ***a***-axis. For the sake of clarity only the tetrahedrally coordinated Si/Al (T) atoms in the framework are shown; oxygen lies approximately at the midpoint of the lines joining the T-sites.

Single crystal investigations are well-suited to problems in which subtle changes in crystal symmetry produce weak reflections or in which complex structures are involved. If sufficiently large single crystals are not available, crystal quality is poor, or diffusion of the sorbate of interest into large single crystals is limited, powders offer a favorable alternative. When only the metric of the unit cell changes, high resolution powder diffraction is particularly useful, as outlined below.

The structures of several sorbate/ZSM-5 complexes have been investigated by both single crystal [20,21,85] and powder diffraction [11,23,86-88]. In those diffraction studies in which small aromatic molecules were absorbed into ZSM-5 [11,20], the location of the sorbate was found to depend on loading. In the most comprehensive of these investigations, Koningsveld et al. [20] found that *p*-xylene was absorbed into both the straight and the sinusoidal channels (Figure 9) at loadings of eight molecules per unit cell. At this loading, the framework undergoes a distortion to $P2_12_12_1$ symmetry. The relationship between these structures is described in detail elsewhere [20].

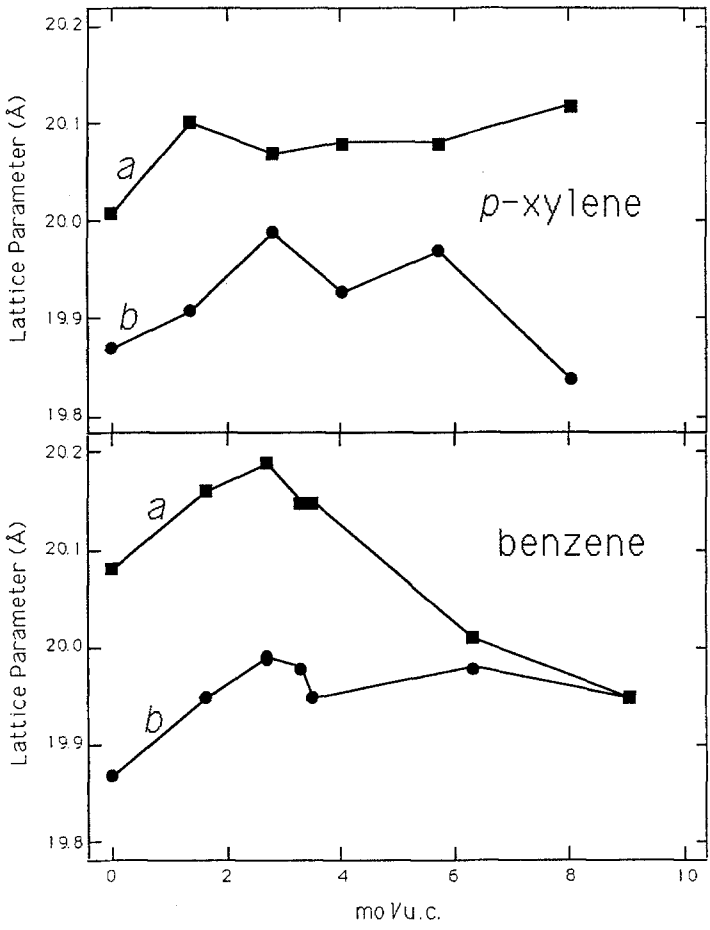

Figure 10. Variation in the ***a*** and ***b*** lattice parameters for ZSM-5 loaded with *p*-xylene (top) and benzene (bottom). Data taken from Kokotailo et al. [81].

3.1 PRELIMINARY INVESTIGATIONS

Initially, attempts were made to load stilbene into single crystals of ZSM-5; the intention being to collect data on a conventional single crystal diffractometer. Unfortunately, the prohibitively slow rates of absorption for stilbene into crystals larger than 50 μm in length necessitated the use of powdered samples. The lattice parameters of crystals exposed to stilbene were found not to have changed; as described below and elsewhere [81], the unit cell parameters are sensitive indicators of the degree of sorption into the ZSM-5 channels.

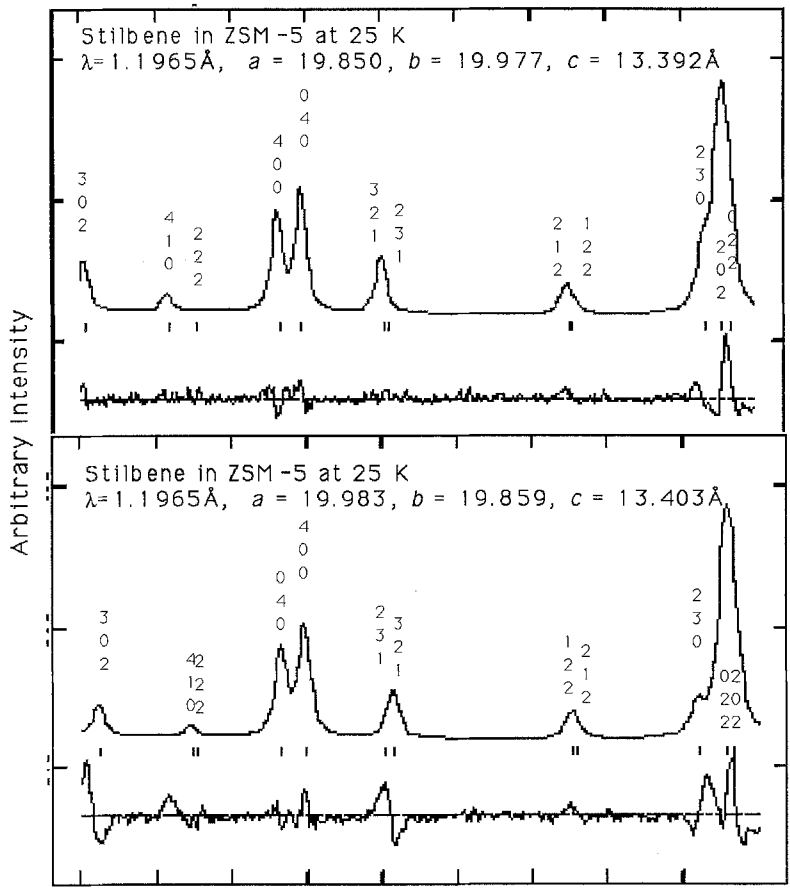

Figure 11. Results of the Le Bail [89] extraction of intensities for two relative settings of the lattice parameters for stilbene loaded in ZSM-5 at 25 K. Refinement from a starting model with $a>b$ converges quickly, but to a clearly inferior fit compared to the model in which $a<b$.

Trans-stilbene was obtained commercially and was recrystallized several times from ethanol. Na,TPA-ZSM-5 was prepared according to the procedure of Rollman and Valyocsik [90]. The stilbene was introduced into a sample with a Si/Al ratio of 550/1 according to the procedure described previously [77,78].

The inevitable loss of information involved in using powder diffraction can be mitigated against by using spectroscopic information in order to constrain composition and degree of order. A thermogravimetric analysis suggested the samples contained 2

molecules of stilbene and one molecule of water per unit cell of ZSM-5. ^{2}H-NMR results [77] suggested little dynamic disorder at room temperature for the sorbed stilbene. This contrasts with the situation in the large-pore zeolite Y, where the NMR results indicate free motion for stilbene; the free diameter for channels in zeolite Y is 7.4 Å while that for the pore is 11 Å [1].

There are several aspects of working with the diffraction data from the stilbene/ZSM-5 complex which are applicable to this class of materials in general. These include the advantages to using high resolution synchrotron X-ray powder diffraction at low temperature and the difficulties involved in interpreting the diffraction data. At room temperature, the unit cell metric for stilbene/ZSM-5 and for other sorbate/ZSM-5 complexes [81] is indistinguishable from tetragonal (Figures 10-13). Prior to beginning a structural study of the stilbene/ZSM-5 complex, it is imperative to determine the relative axial lengths of the unit cell. At room temperature, this is not straight-forward (Figures 10,13). The assignment of the proper space group can also be impaired by the incorrect assignment of the unit cell lengths; the distinction between ***Pnma*** and ***P2$_1$2$_1$2$_1$*** [20] depends on the presence or absence of weak reflections of the type *0kl; k+l* = 2*n*+1 and *h0l; h* = 2*n*+1. Being able to correctly predict the position of such peaks in the powder diffraction pattern is an indispensable aid to their location, should they exist.

The correct assignment of lattice parameters is greatly aided by the use of the Le Bail technique [89], a simple modification of the procedure proposed by Rietveld [66]. This method has been used to extract intensity information for the ab initio determination of crystal structure [89,91]. The procedure does not require any structural model. Instead, an arbitrary set of calculated structure factors is input and only the appropriate profile parameters refined; this might include lattice parameters, diffractometer zero, and parameters to describe peak shape [67]. From the initially calculated values, a set of I(*hkl*) values is generated by dividing the observed intensity at each data point in a step-scan profile in the ratio of the calculated contributions of individual *hkl*'s to that point. These points are summed for an individual *hkl* to obtain an integrated intensity for that reflection and then input as calculated values and the least squares process is repeated until convergence is achieved. If the individual peaks are well separated (Figure 11), this is a rapid process since the correlations between parameters is unimportant. On the other hand, when, as in the case of ZSM-5 at room temperature (Figures 12,13), peaks are not well-resolved, they will tend to be assigned similar intensities; the relative lengths of the lattice parameters must then be decided on the basis of weak intensities which unambiguously distinguish between models in which the ***a***-axis is longer than ***b*** , and one in which ***a*** < ***b***.

3.2 VARIATION IN UNIT CELL OF STILBENE/ZSM-5 WITH TEMPERATURE

The diffraction experiments were performed in high resolution mode [6,16] at the NSLS on beamlines X-7A and X-3B. In order to follow changes in the unit cell with temperature, the sample was loaded into a quartz capillary of 1 mm OD and placed first

in a Displex® closed-cycle refrigerator fitted with a Be window for measurement from 20 to 280 K. A cylindrical furnace [92,93] was used for measurements from 300 K to 450 K. Step scans were carried out over selected angular regions covering the (*110*), (*020/200*), (*321/231*), (*040/400*), and (*410*) reflections at several temperatures (Figures 12 and 13). At about 440 K, stilbene was lost from the sample. The wavelengths used for the experiments were obtained by calibration with a reference sample of CeO_2 (***a*** = 5.4113Å).

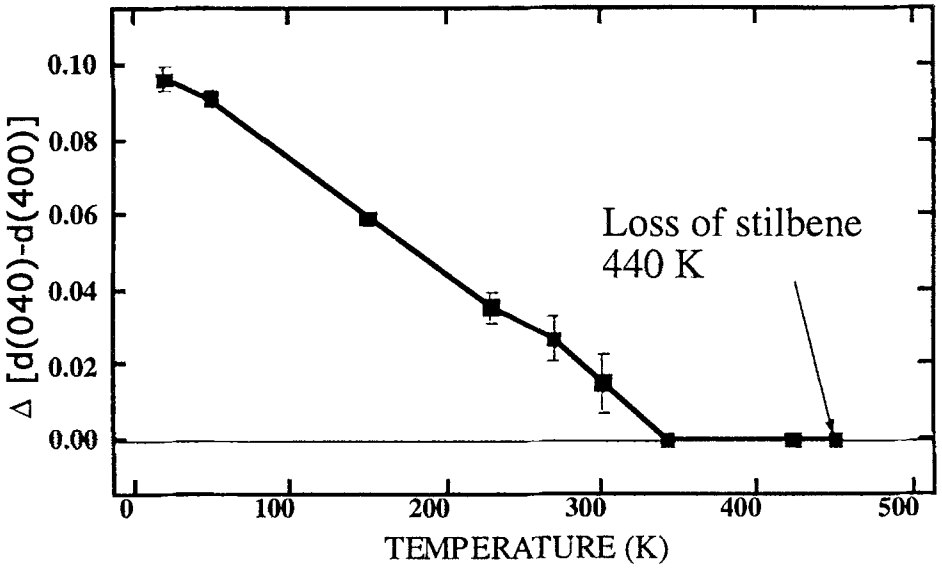

Figure 12. Variation in the splitting of the (*040*)-(*400*) reflections, shown in Figure 13, as a function of temperature. The wavelength, determined from the CeO_2 standard, is 1.1965Å.

Diffraction data for the (*040/400*) pair of reflections along with the (*410*) are reproduced in Figure 13 to show the relative changes in the ***a***- and ***b***-axes in the temperature range 25 K to 300 K. The assignment of the (*040*) to the lower angle peak in the (*040/400*) pair is made on the basis of the final Rietveld refinement described below. The assignment at the higher temperatures was made on the basis of the Le Bail extraction [89]. The relative lengths of the ***a***- and ***b***-axes is unusual in that other orthorhombic cells reported for ZSM-5 [4,18,20,21,23,80,81,83,84,86-88,94,95] have $a > b$. It should be noted that, because of the pseudo-tetragonal metric for this material, the position of a few weak reflections of the type *hk0; h* = 2*n* help to define the unit cell (Figure 11). With laboratory-based diffractometers, these reflections can be easily lost in the background or appear as poorly resolved shoulders (Figure 11). This situation is exacerbated at room temperature where, even with the superior resolution afforded by the

X-7A diffractometer, the ***a*** unit cell parameter is indistinguishable from ***b*** (Figures 12 and 13). In this case, Rietveld refinement [66,67,89] is required to resolve the ambiguity.

At 25 K, the orthorhombic nature of the cell is clearly evident (Figure 13). Further, there is no broadening of the (*111*), which would indicate monoclinic symmetry; the diffraction pattern was fully indexed on the basis of an orthorhombic cell (***a*** = 19.8526(1), ***b*** = 19.9801(2) and ***c*** = 13.3921(2) Å) with absences corresponding to diffraction symmetry ***Pn-a***. The mirror plane perpendicular to the ***b***-axis was assumed throughout the subsequent investigations; there was no diffraction evidence for the space group $P2_12_12_1$. Upon warming to room temperature, the cell derived from a preliminary Rietveld-type refinement was ***a*** = 19.9601(2), ***b*** = 19.9907(2) and ***c*** = 13.4155(2) Å; this represents a linear expansion of 0.54%, 0.05% and 0.17% along ***a***, ***b***, and ***c***, respectively.

3.3 THE STRUCTURE OF THE STILBENE/ZSM-5 COMPLEX

More extensive X-ray data were collected at 25 K at a wavelength of 1.1965 Å and with beam defining slits 1.1 mm by 8.0 mm. A Ge(111)/Ge(220) monochromator/analyzer with a Kevex® detector was used [6,16]. Data were collected from 5° to 70° in 2θ with a step size of 0.008° in 2θ and a counting time of 4 sec for low angle and 5 sec for data above 30°. The low angle portion of the extended data set was used in a molecular modeling study; this section of the diffraction pattern is more sensitive to the location of the lighter hydrocarbon molecule in the silicate framework (Figure 14) than the higher angle data. Initially the silicate framework was optimized using distance least squares (DLS) based on known interatomic distances [69] and the lattice parameters derived from a Le Bail-type [89] refinement. The unit cell contents were fixed at two molecules of stilbene per unit cell (an occupancy of 0.25 per general position in ***Pnma***) consistent with results of thermogravimetric measurements.

Final adjustments were carried out to give a good visual fit between observed and calculated patterns and the positional parameters for the framework atoms and sorbate molecule (Figure 14) were exported for further refinement using GSAS [67]. The positional parameters for the framework were adjusted using the Rietveld method [66]; the diffraction data were supplemented with 107 inter-atomic T-O, O-O and T-T distances taken from the recent accurate single crystal study of orthorhombic ZSM-5 loaded with *para*-xylene [20]. For the final refinement the positions of all framework atoms were varied while their thermal parameters and all parameters for the stilbene were fixed. The diffractometer zero, lattice parameters, and 5 profile coefficients [67] were also varied. Figure 15 gives a graphical representation of the fit in the low-angle region of the 25 K data and the model is given in Table 5. The usual discrepancy indices were R_{wp} = 0.185 and χ^2 = 3.2. The background was estimated at points between the diffraction maxima (Figure 15).

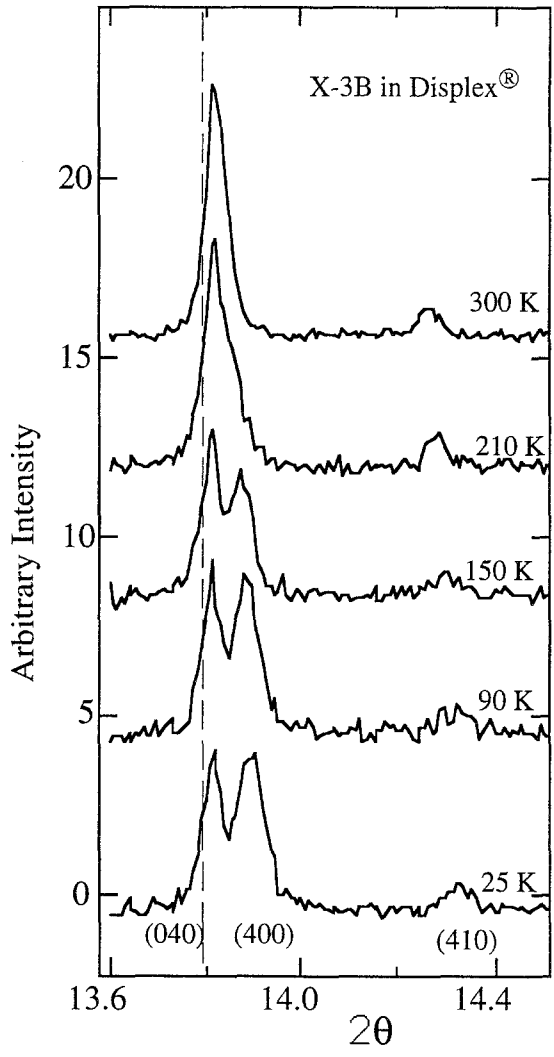

Figure 13. Synchrotron X-ray scans through the (*040/400*) and (*410*) reflections from stilbene-loaded ZSM-5 as a function of temperature at a wavelength 1.1956Å on the X-3B beamline. The (*140*) reflection, absent for diffraction symbol ***Pn-a,*** is not observed. It would appear just to the low angle side of the (*410*) reflection. Note that the ***a***-axis (Figure 9) is almost invariant with temperature.

Table 5. Refined framework* parameters and positions of atoms in stilbene in the ZSM-5/stilbene complex.

atom	*x*	*y*	*z*	atom	*x*	*y*	*z*
T1	0.4211(4)	0.0553(5)	-0.3514(6)	O16	0.4163(7)	0.1246(7)	-0.410(1)
T2	0.2993(4)	0.0288(4)	-0.2102(6)	O17	0.4103(6)	-0.0042(8)	-0.4281(9)
T3	0.2818(4)	0.0626(4)	0.0143(5)	O18	0.4053(9)	-0.1324(5)	-0.4407(8)
T4	0.1241(5)	0.0647(5)	0.0148(6)	O19	0.1783(6)	0.1275(4)	-0.4076(7)
T5	0.0707(5)	0.0270(4)	-0.1934(5)	O20	0.1863(8)	-0.0006(4)	-0.429(1)
T6	0.1775(4)	0.0578(4)	-0.3503(6)	O21	0.1895(9)	-0.1295(3)	-0.4383(8)
T7	0.4209(6)	-0.1719(2)	-0.3404(8)	O22	-0.0057(5)	0.0500(7)	-0.1964(7)
T8	0.3001(5)	-0.1292(4)	-0.2052(6)	O23	-0.0053(6)	-0.155(1)	-0.1969(9)
T9	0.2801(6)	-0.1734(2)	0.0174(5)	O24	0.4147(9)	-0.250	-0.360(1)
T10	0.1238(6)	-0.1738(2)	0.0183(8)	O25	0.1777(8)	-0.25	-0.3711(9)
T11	0.0707(5)	-0.1309(4)	-0.1914(7)	O26	0.296(1)	-0.25	0.0397(9)
T12	0.1790(6)	-0.1734(9)	-0.3407(7)	O27	0.109(1)	-0.25	0.0462(9)
O1	0.3670(6)	0.0497(8)	-0.264(1)	C1	1.030	-0.593	-0.522
O2	0.2986(8)	0.0596(7)	-0.1010(6)	C2	1.024	-0.519	-0.518
O3	0.2029(4)	0.063(1)	0.030(1)	C3	1.045	-0.481	-0.592
O4	0.1071(6)	0.0606(8)	-0.1006(6)	C4	1.052	-0.412	-0.589
O5	0.1079(5)	0.0493(7)	-0.2931(6)	C5	1.028	-0.381	-0.511
O6	0.2370(6)	0.0565(8)	-0.272(1)	C6	0.988	-0.418	-0.438
O7	0.3685(7)	-0.1505(9)	-0.257(1)	C7	0.991	-0.487	-0.441
O8	0.3002(8)	-0.1563(6)	-0.0940(5)	C8	1.005	-0.629	-0.444
O9	0.2021(6)	-0.1602(8)	0.0329(9)	C9	1.009	-0.703	-0.447
O10	0.1055(7)	-0.1627(6)	-0.0960(8)	C10	0.988	-0.740	-0.366
O12	0.1097(8)	-0.1541(9)	-0.2891(8)	C11	0.990	-0.809	-0.370
O13	0.2388(8)	-0.1602(8)	-0.265(1)	C12	1.014	-0.840	-0.454
O14	0.2944(9)	-0.0502(4)	-0.204(1)	C13	1.045	-0.803	-0.535
O15	0.0737(9)	-0.0519(4)	-0.183(1)	C14	1.033	-0.734	-0.532

* ***Pnma***, a = 19.86537, b = 19.99053, c = 13.40364.

Real-time calculation of the powder pattern, as stilbene was positioned within the channels of a rigid framework, showed clearly the molecule was absorbed into the straight-channel (Figure 14) rather than the sinusoidal channels. Translation along the straight-channel located the molecule with one phenyl ring close to the intersection of the straight- and sinusoidal-channels (Figures 9 and 14) and the other at y = $^1/_2$. This is close to the position found for *para*-dichlorobenzene [11].

The refinement shows that stilbene, at a loading of two molecules per unit cell, is located with one phenyl ring close to the mirror planes at y = $^1/_4$ and $^3/_4$ at the

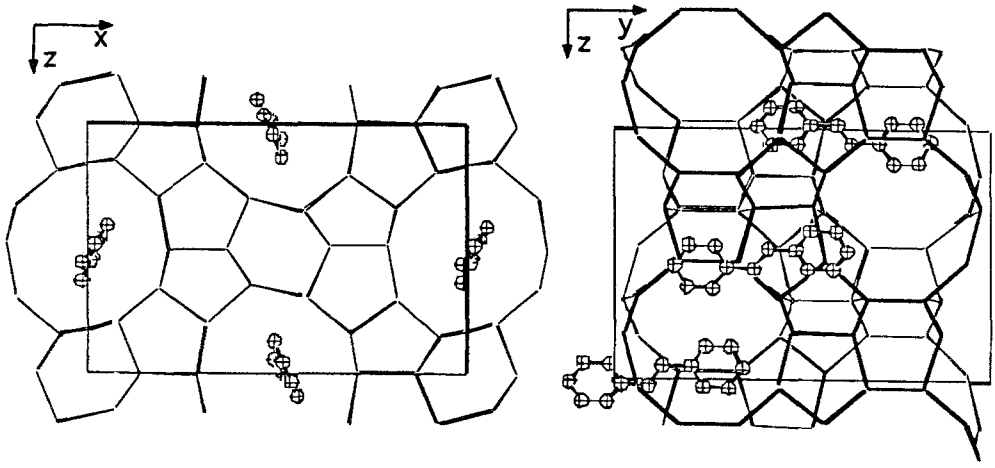

Figure 14. Projection of the structure of the ZSM-5/stilbene complex at 25 K along the ***b***-axis (left) and the ***a***-axis (right) The position of the sorbate molecule, *trans*-stilbene, is that obtained from the structure modeling procedure (see text). For clarity, only selected orientations of the molecule, which is disordered about the mirror planes at $y = 1/4$ and 3/4, are shown.

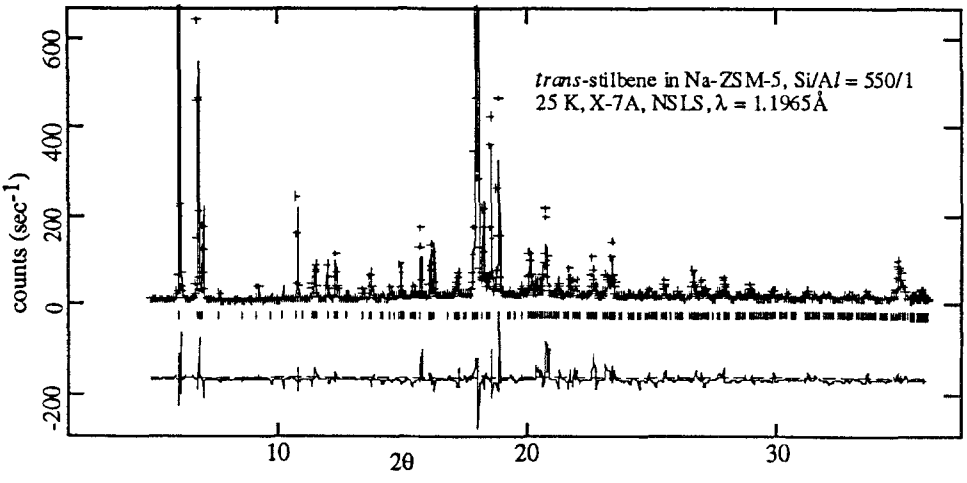

Figure 15. Calculated (line) and observed X-ray powder diffraction profiles for *trans*-stilbene (occupancy = 0.25) in Na-ZSM-5. The difference pattern is given below. Note that the intensity is truncated at 600 counts normalized to 100 mA. The strongest peak in the pattern, the (*011*), has an intensity of 1500 counts.

intersections of the straight and sinusoidal channels; the center of the molecule (Figure 14) is located at a general position at $x = 1.02$, $y = -0.611$, and $z = -0.483$. The molecules shown in Figure 14 represent one of two possible orientations about the mirrors. This disorder is apparently static since NMR experiments suggest little dynamic disorder, even at room temperature [77]. The second phenyl ring (Figure 14) is located at a position in the straight channel where contacts between the sorbate and the framework are maximized. This position is apparently favored by *para*-xylene at low loadings [11]. Refinement of the framework positional parameters also suggests an elliptical distortion of the 10-rings, constituting the straight-channels, in response to the absorption of the two molecules of stilbene.

Acknowledgments

This work has benefited greatly from the financial and moral support of collaborators at The DuPont Company. These include Drs. L. Abrams, J. Calabrese, D. Corbin, R. Harlow, G. Jones and M. Smith (University of Delaware). Additional financial support from NSF grant DMR-90-24249 is much appreciated. The X-7A and X-3 beamlines at the NSLS, Brookhaven National Laboratory, are supported by the DOE. The diffraction work reported here owes much to my fellow X-7 Participating Research Team (PRT) members at X-7A: L. Finger, J. Hriljac, B. Toby, and most particularly David Cox who, through his singular skill in building and developing X-7A, has demonstrated how productive the PRT concept can be.

References

1. W. M. Meier and D. H. Olson, *Atlas of Zeolite Structure Types*, Butterworths, London (1987).
2. P. B. Weisz and V. J. Frilette, *J. Phys. Chem.*, **64**, 382 (1960).
3. V. Alfredsson, T. Ohsuna, O. Terasaki, and J. Bovin, *Angew. Chem. Int. Ed. Engl.*, **32**, 1210 (1993).
4. J. J. Pluth and J. V. Smith, in *Intrazeolite Chemistry*, G. D. Stucky and F. G. Dyer (Eds), *ACS. Symp. Ser.* **218**, 119 (1983).
5. W. M. Meier, in *Zeolites: Synthesis, Structure, Technology and Application*, B. Drzaj, S. Hocevar, and S. Pejovnik (Eds), *Stud. Surf. Sci. Catal.*, **24**, 217 (1985).
6. D. E. Cox, B. H. Toby, and M. M. Eddy, *Aust. J. Phys.*, **41**, 117 (1988).
7. L. E. Iton, F. Trouw, T. O. Brun, J. E. Epperson, J. W. White, and S. J. Henderson, *Langmuir*, **8**, 1045 (1992).
8. J. Newsam and D. E. W. Vaughan, in *Zeolites: Synthesis, Structure, Technology and Application*, B. Drzaj, S. Hocevar, and S. Pejovnik (Eds), *Stud. Surf. Sci. Catal.*, **24** (1985).
9. J. M. Newsam, *Mat. Sci. Forum*, **27-28**, 385 (1987).

10. C. A. Fyfe, H. Stobl, H. Gies, G. T. Kokatailo, and G. Barlow, *J. Am. Chem. Soc*, **66**, 1942 (1988).
11. H. Gies, B. Marler, C. Fyfe, G. Kokotailo, Y. Feng, and D. E. Cox, *J. Phys. Chem. Solids*, **52**, 1235 (1991).
12. C. R. A. Catlow and C. M. Freeman, *Royal Institution Proceedings*, **63**, 51 (1992).
13. J. M. Newsam, in *Proceedings of the Ninth International Zeolite Conference*, R. B. v. Ballmoos, J. B. Higgins, and M. M. J. Treacy (Eds), Butterworth-Heineman, London, p 127 (1992).
14. A. P. Wilkinson, A. K. Cheetham, S. C. Tang, and W. J. Reppart, *J. Chem. Soc., Chem. Comm.*, 1485 (1992).
15. P. Coppens, *Synchrotron Radiation Crystallography*, Academic Press, London, (1992).
16. D. E. Cox, in *Synchrotron Radiation Crystallography*, P. Coppens (Eds), Academic Press, London, Vol. 186 (1992).
17. J. J. Pluth and J. V. Smith, in *8th International Zeolite Conference*, P. A. Jacobs and R. A. van Santen (Eds), Vol. 49, p 835 (1989).
18. H. v. Koningsveld, J. C. Jensen, and H. v. Bekkum, *Zeolites*, **10**, 235 (1990).
19. H. v. Koningsveld, J. C. Jensen, and H. v. Bekkum, *Zeolites*, **9**, 253 (1989).
20. H. v. Koningsveld, F. Tuinstra, H. v. Bekkum, and J. C. Jensen, *Acta Crystallog.*, **B45**, 423 (1989).
21. H. v. Koningsveld, F. Tuinstra, H. v. Bekkum, and J. C. Jensen, *Acta Crystallog.*, **B45**, 127 (1989).
22. H. v. Koningsveld, J. C. Jensen, and H. v. Bekkum, *Zeolites*, **7**, 564 (1987).
23. B. F. Mentzen and M. Sacerdote-Peronnet, *Mat. Res. Bull.*, **28**, 1161 (1993).
24. D. L. Bish and J. E. Post, *Modern Powder Diffraction*, Mineralogical Society of America, Washington, DC (1989).
25. G. C. Smith, *Synch. Rad. News*, **4**, 24 (1991).
26. P. A. Lee, P. H. Citrin, P. Eisenberger, and B. M. Kincaid, *Rev. Mod. Phys*, **53**, 769 (1981).
27. J. B. Parise, J. E. MacDougall, N. Herron, R. Farlee, A. W. Sleight, Y. Wang, T. Bein, K. Moller, and L. M. Moroney, *Inorg. Chem.*, **27**, 221 (1988).
28. G. A. Ozin, M. R. Steele, and A. J. Holmes, *Chem. Mater.*, **6**, 999 (1994).
29. C. J. Drummond and B. W. Ninham, *Chem. Aust.*, **59**, 529 (1992).
30. J. M. Newsam, T. O. Brun, F. Trouw, L. E. Iton, and Curtiss, in *New Catalytic Materials and Techniques*, R. T. K. Baker and L. L. Murrell (Eds), *ACS. Symp. Series* **437**, 25 (1990).
31. W. H. Baur, R. X. Fischer, R. D. Shannon, R. H. Staley, A. J. Vega, L. Abrams, D. R. Corbin, and J. D. Jorgensen, *Z. Kristallogr.*, **179**, 281 (1987).
32. W. H. Baur, R. X. Fischer, and R. D. Shannon, in *Innovation in Zeolite Materials Science*, P. J. Grobet (Ed), Elsevier, Amsterdam p 281 (1988).
33. W. H. Baur, A. Bieniok, R. D. Shannon, and E. Prince, *Z. Kristallogr.*, **187**, 253 (1989).
34. A. Bieniok and W. H. Baur, *J. Solid State Chem.*, **90**, 173 (1991).

35. A. Bieniok and W. H. Baur, *Mat. Sci. Forum*, **79-82**, 721 (1991).
36. A. Bieniok and W. H. Baur, *Acta Cryst.*, **B49**, 812 (1993).
37. D. R. Corbin, L. Abrams, G. A. Jones, M. M. Eddy, W. T. A. Harrison, G. D. Stucky, and D. E. Cox, *J. Amer. Chem. Soc.*, **112**, 4821 (1990).
38. D. R. Corbin, L. Abrams, G. A. Jones, T. E. Gier, R. L. Harlow, J. B. Parise, and P. J. Dunn, in *Synthesis/Characterization and Novel Applications of Molecular Sieve Materials*, R. L. Bedard, T. Bein, M. E. Davis, J. Garces, V. A. Maroni, and G. D. Stucky (Eds), Materials Research Society, Pittsburgh, PA, p 23 (1990).
39. D. R. Corbin, L. Abrams, G. A. Jones, M. M. Eddy, W. T. A. Harrison, G. D. Stucky, and D. E. Cox, *J. Amer. Chem. Soc.*, **112**, 4821 (1990).
40. R. X. Fischer, W. H. Baur, R. D. Shannon, R. H. Staley, A. J. Vega, L. Abrams, and E. Prince, *J. Phys. Chem.*, **90**, 4414 (1986).
41. R. X. Fischer, W. H. Baur, R. D. Shannon, R. H. Staley, A. J. Vega, L. Abrams, D. R. Corbin, and J. D. Jorgensen, *Z. Kristallogr.*, **179**, 281 (1987).
42. R. X. Fischer, W. H. Baur, R. D. Shannon, R. H. Staley, L. Abrams, A. J. Vega, and J. D. Jorgensen, *Acta Cryst.*, **B44**, 321 (1988).
43. R. X. Fischer, W. H. Baur, and R. D. Shannon, *Acta Cryst.*, **C45**, 983 (1989).
44. L. B. McCusker, and C. Baerlocher, in *Sixth International Zeolite Conference*, D. Olson and A. Bisio (Eds), Butterworths, London, p 812 (1984).
45. L. B. McCusker, *Zeolites*, **4**, 51 (1984).
46. J. B. Parise, and E. Prince, *Mat. Res. Bull.*, **18**, 841 (1983).
47. J. B. Parise, L. Abrams, T. E. Gier, D. R. Corbin, J. D. Jorgensen, and E. Prince, *J. Phys. Chem.*, **88**, 2303 (1984).
48. J. B. Parise, T. E. Gier, D. R. Corbin, and D. E. Cox, *J. Phys. Chem.*, **88**, 1635 (1984).
49. J. B. Parise, X. Liu, D. R. Corbin, and G. A. Jones, in *Synthesis/Characterization and Novel Applications of Molecular Sieve Materials*, R. L. Bedard, T. Bein, M. E. Davis, J. Garces, V. A. Maroni, and G. D. Stucky (Eds), Materials Research Society, Pittsburgh, PA, p 267 (1991).
50. J. B. Parise, X. Liu, and D. R. Corbin, *J. Chem. Soc., Chem. Commun.*, **3**, 162 (1991).
51. J. B. Parise, D. R. Corbin , L. Abrams, P. Northrup, J. Rackovan, T. M. Nenoff, and G. Stucky, *Zeolites*, **14**, 24 (1993).
52. A. V. Vernov, W. A. Steele, and L. Abrams, *J. Phys. Chem.*, **97**, 7660 (1993).
53. A. Loriso, M. J. Bojan, A. Vernov, and W. A. Steele, *J. Phys. Chem.*, **97**, 7665 (1993).
54. C. -J. Tsiao, J. S. Kauffman, D. R. Corbin, L. Abrams, E. Carroll, and C. Dybowski, *J. Phys. Chem*, **95**, 5586 (1991).
55. P. A. Wright, J. M. Thomas, S. Ramdas, and A. K. Cheetham, *J. Chem. Soc., Chem. Comm.*, 1338 (1984).
56. M. L. Smith, D. R. Corbin, and C. Dybowski, *J. Phys. Chem.*, **97**, 9045 (1993).
57. R. Rinaldi, J. J. Pluth, and J. V. Smith, *Acta Cryst.*, **B31**, 1603 (1975).
58. J. L. Schlenker, J. J. Pluth, and J. V. Smith, *Mat. Res. Bull.*, **14**, 751 (1979).

59. J. L. Schlenker, J. J. Pluth, and J. V. Smith, *Mat. Res. Bull.*, **14**, 849 (1979).
60. W. J. Mortier, J. J. Pluth, and J. V. Smith, *Nature*, **256**, 718 (1975).
61. W. J. Mortier, *Comparison of Extraframework Sites in Zeolites*, Butterworths, London (1983).
62. I. Gameson, P. A. Wright, T. Rayment, and J. M. Thomas, *Chem Phys. Lett.*, **123**, 145 (1986).
63. M. Keane Jr., G. C. Sonnichsen, L. Abrams, D. R. Corbin, T. E. Gier, and R. D. Shannon, *Appl. Catal.*, **32**, 361 (1987).
64. T. E. Gier, R. D. Shannon, G. C. Sonnichsen, D. R. Corbin, and M. Keane, Jr., *US Patent 4,806,689* (1989).
65. T. Ito and J. Fraissard, *Zeolites*, **7**, 554 (1987).
66. H. M. Rietveld, *J. Appl. Crystallog.*, **2**, 65 (1969).
67. A. C. Larson and R. B. Von Dreele, *GSAS: General Structure Analysis System,* Los Alamos Nat. Lab., Rpt. No.:LAUR86-748 (1986)
68. R. X. Fisher, W. H. Baur, R. D. Shannon, R. H. Staley, L. Abrams, A. Vega, and J. Jorgensen, *Acta Cryst.*, **B44**, 321 (1988).
69. C. Baerlocher, A. Hepp, and W. M. Meier, *DLS Manual*, Institut für Kristallographie und Petrographie: ETH, Zurich (1977).
70. D. R. Corbin, L. Abrams, M. L. Smith, C. R. Dybowski, J. B. Parise, and J. Hriljac, *J. Chem. Soc., Chem. Comm*, 1027 (1993).
71. H. E. Robson, D. P. Shoemaker, R. A. Ogilvie, and P. C. Manor, *ACS. Advan. Chem. Series*, **121**, 106 (1973).
72. H. E. Robson, *U.S. Patent 3,904,738* (1975).
73. N. J. Turro and P. Wan, *J. Am. Chem. Soc.*, **107**, 678 (1985).
74. N. J. Turro and Z. Zhang, *Tetrahedron Letters*, **28**, 5637 (1987).
75. N. J. Turro, X. Lei, and C. -C. Cheng, *J. Am. Chem. Soc.*, **107**, 5824 (1985).
76. J. V. Caspar, V. Ramamurthy, and D. R. Corbin, *J. Am. Chem. Soc.*, **113**, 600 (1991).
77. V. Ramamurthy, J. V. Caspar, D. R. Corbin, D. F. Eaton, J. S. Kauffman, and C. Dybowski, *J. Photochem. Photobiol*, **31**, 47 (1990).
78. V. Ramamurthy, J. V. Caspar, and D. R. Corbin, *J. Am. Chem. Soc.*, **113**, 594 (1991).
79. H. Nakamoto and H. Takahashi, *Chem. Letters*, 1013 (1981).
80. D. G. Hay and H. Jaeger, *J. Chem. Soc., Chem. Comm.*, 1433 (1984).
81. G. Kokotailo, L. Riekert, and A. Tissler, in *Zeolites as Catalysts, Sorbents and Detergent Builders*, H. G. Karge and J. Weitkamp (Eds), Elsevier Scientific, Amsterdam, p 821 (1989).
82. J. B. Parise, J. A. Hriljac, D. E. Cox, D. R. Corbin, and V. Ramamurthy, *J. Chem. Soc., Chem. Comm.*, 226 (1993).
83. J. Taylor, *Zeolites*, **7**, 311 (1987).
84. E. L. Wu, S. L. Lawton, D. H. Olson, A. C. Rohman, and G. T. Kokotailo, *J. Phys. Chem.*, **83**, 2777 (1979).
85. G. D. Price, J. J. Pluth, J. V. Smith, and T. Araki, *Nature*, **292**, 818 (1981).

86. C. Baerlocher, in *Proceedings of the 6th International Zeolite Conference*, D. Olson and A. Bisio (Eds), Butterworths, Guildford, UK, p 823 (1984).
87. B. F. Mentzen, *Mat. Res. Bull.*, **22**, 489 (1987).
88. B. F. Mentzen, *J. Appl. Crystallog.*, **22**, 100 (1989).
89. A. Le Bail, H. Duroy, and J. L. Fourquet, *Mat. Res. Bull.*, **23**, 447 (1988).
90. L. S. Rollman and E. K. Volyocsik, *Inorganic Syntheses*, Wiley, New York, **22**, 61-68 (1983).
91. J. A. Hriljac, J. B. Parise, G. H. Kwei, and K. B. Schwartz, J. *Phys. Chem. Solids*, **52**, 1273 (1991).
92. Y. Zhao, D. J. Weidner, J. B. Parise, and D. E. Cox, *Phys. Earth Planet. Inter.*, **76**, 1 (1993).
93. Y. Zhao, D. J. Weidner, J. B. Parise, and D. E. Cox, *Phys. Earth Planet. Inter.*, **76**, 17, (1993).
94. E. R. Geus, M. J. Den Exter, and H. v. Bekkum, *J. Chem. Soc., Faraday Trans*, **88**, 3101 (1992).
95. D. H. Olson, W. O. Hagg, and R. M. Lago, *J. Catal.*, **61**, 390 (1980).

Abstract. The development and increased availability of brighter synchrotron sources has stimulated investigations of zeolite-inclusion complexes using powder X-ray diffraction data. This is illustrated with two examples of studies facilitated by these sources. Both involve the use of Rietveld refinement to obtain structure from data collected at a versatile synchrotron beamline. The first example describes the structural changes commensurate with Xe desorption from a fully Xe-loaded powder sample of Cd-exchanged zeolite rho. After exposure to the atmosphere, data were collected in real-time as Xe desorbed from the sample over a four hour period. The results of Rietveld refinement indicate that Xe is not lost continuously; instead within the first hour, Xe desorbs completely from the 8-ring and is replaced by H_2O. Following rearrangement of the remaining Xe between the available 6-ring sites, it is lost as the sample hydrates fully. This behavior is probably the result of competition with H_2O, which prefers the 8-ring site. In the second example, the high resolution and signal-to-background discrimination afforded the synchrotron powder X-ray diffraction experiment, was used to advantage to study the stilbene-ZSM-5 complex. Stilbene was located, using modeling techniques, in the straight channels with one phenyl ring at the intersection of the two channel system. The structure is pseudo-tetragonal (*a a b*) at room temperature but distorts at lower temperatures to give $b > a$. Distinguishing these subtle structural changes is facilitated by the superior resolution available at a beamline configured with both incident and diffracted beam monochromators.